ANNUAL REVIEWS

Annual Review of Nuclear and Particle Science

Exploring Stars in Underground Laboratories: Challenges and Solutions

Marialuisa Aliotta,[1] Axel Boeltzig,[2,3] Rosanna Depalo,[4,5] and György Gyürky[6]

[1]SUPA, School of Physics and Astronomy, University of Edinburgh, Edinburgh, United Kingdom; email: m.aliotta@ed.ac.uk

[2]Department of Physics, Università degli Studi di Napoli Federico II, Napoli, Italy

[3]Institute of Nuclear Physics, Helmholtz-Zentrum Dresden-Rossendorf, Dresden, Germany

[4]Department of Physics, Università degli Studi di Milano, Milano, Italy

[5]Istituto Nazionale di Fisica Nucleare Milano, Milano, Italy

[6]Institute for Nuclear Research, Hungarian Academy of Sciences, Debrecen, Hungary

Annu. Rev. Nucl. Part. Sci. 2022. 72:177–204

First published as a Review in Advance on July 8, 2022

The *Annual Review of Nuclear and Particle Science* is online at nucl.annualreviews.org

https://doi.org/10.1146/annurev-nucl-110221-103625

Keywords

stellar evolution, nucleosynthesis, nuclear astrophysics experiments, background suppression underground

Abstract

For millennia, mankind has been fascinated by the marvel of the starry night sky. Yet, a proper scientific understanding of how stars form, shine, and die is a relatively recent achievement, made possible by the interplay of different disciplines as well as by significant technological, theoretical, and observational progress. We now know that stars are sustained by nuclear fusion reactions and are the furnaces where all chemical elements continue to be forged out of primordial hydrogen and helium. Studying these reactions in terrestrial laboratories presents serious challenges and often requires developing ingenious instrumentation and detection techniques. Here, we reveal how some of the major breakthroughs in our quest to unveil the inner workings of stars have come from the most unexpected of places: deep underground. As we celebrate 30 years of activity at the first underground laboratory for nuclear astrophysics, LUNA, we review some of the key milestones and anticipate future opportunities for further advances both at LUNA and at other underground laboratories worldwide.

Contents

1. INTRODUCTION

Much of what we know about the makeup of the Universe stems from the study of the electromagnetic radiation emitted by stars, galaxies, the interstellar medium, and the early Universe some 380,000 years after the big bang. Stellar spectra, in particular, provide a wealth of information about the physical properties of a star's outermost layers: Like cosmic bar codes, their dark absorption lines[1] reveal the chemical composition of the gas clouds out of which a star formed.

Over the past decades, ground-based and space-borne telescopes have opened up unprecedented opportunities to observe the Universe at virtually all wavelengths, from radio frequencies to X- and γ-ray energies. More recently, the direct detection of gravitational waves (disturbances in the curvature of space-time) resulting from colliding neutron stars and/or black holes has marked the birth of a multi-messenger era in astronomical observations (1, 2). Other direct messengers

[1]Absorption lines are caused by the absorption of the radiation emitted by a star at specific frequencies characteristic of the chemical elements present in the stellar atmosphere.

come in the form of tiny amounts of matter that reach the Earth from outer space, such as cosmic rays (highly energetic charged particles), presolar grains found in meteorite samples, and neutrinos (from both the Sun and nearby supernovae). Like pieces of a cosmic jigsaw puzzle, these sources of information reveal a tremendous diversity of cosmic objects but also point to a striking feature of the Universe as a whole: 98% of all visible matter consists of hydrogen and helium, with all other chemical elements (collectively called metals) making up a mere 2%!

And yet, where do these elements come from? How, when, and where were they forged? In an attempt to answer these questions, in 1957, Burbidge, Burbidge, Fowler, and Hoyle (3), and independently Cameron (4), laid the foundations of nuclear astrophysics, a vibrant interdisciplinary field that brings together astronomy and nuclear, atomic, and plasma physics, and requires efforts in observations, theory, and experiments. The framework suggested to explain the origin of the chemical elements and their abundance distribution in the Universe has stood the test of time, through a wealth of astronomical observations and experimental verification.

Starting from protons and neutrons, the key building blocks produced during the big bang, all other elements are created via complex patterns of nuclear reactions. Some occurred within the first few minutes of life of the Universe and led to the synthesis of ^{2}H (deuterium), ^{3}He, and ^{4}He, as well as traces of Li, Be, and B. As the Universe continued to expand, nucleosynthesis halted for a few hundred million years, until the first stars (and galaxies of stars) started to emerge from the gravitational contraction of vast molecular clouds. In the hot interiors of stars, heavier elements were finally produced (and are still produced today) through sequences of fusion reactions between charged particles, starting from H and He. As the binding energy per nucleon increases as a function of mass number up to a maximum in the Fe mass region ($A \sim 60$), nuclear fusion liberates energy and stabilizes a star against further contraction. However, fusion beyond Fe becomes energetically disfavored, and different reaction mechanisms must be invoked to explain the origin of elements heavier than Fe. These mechanisms involve a sequence of slow or rapid neutron capture processes (the s- and r-processes, respectively) followed by β^- decays, where an excess neutron in a nucleus is converted into a proton, thus leading to a new chemical element.

Like gigantic cauldrons in the cosmos, stars are therefore responsible for cooking all elements out of primordial ingredients, H and He. Eventually, more massive stars end their lives in catastrophic supernova explosions, thus ejecting back into the interstellar medium all the new elements created in their interiors. In turn, new generations of stars, born out of this enriched cosmic soup, will also contribute to the chemical evolution of the Universe, in a continuous recycling of stellar material.

From these general considerations, nuclear physics and nuclear properties emerge to take center stage in the description of the chemical evolution of stars, galaxies, and, ultimately, the Universe. A key goal of nuclear astrophysics consists of replicating in the laboratory the nuclear reactions that take place in stars, so as to better understand the intricate pattern of processes that have led to the distribution of abundances that we observe today. Unfortunately, because of the relatively small energies at which nuclear reactions take place in stars, measuring their cross sections—i.e., the probability for a reaction to occur—poses formidable challenges to experimenters.

In this review, we briefly recall the main features of thermonuclear reactions in stars to illustrate the challenges and requirements related to their study in terrestrial laboratories. We then show how performing experiments in underground laboratories has proved essential not just when studying reactions that liberate γ-rays, but also those that emit neutrons or charged particles. Following the pioneering work performed at the first ever Laboratory for Underground Nuclear Astrophysics (LUNA), we celebrate its legacy 30 years on as we look forward to future opportunities, both at LUNA and elsewhere, to unveil some of the best-kept secrets of nature.

2. NUCLEAR REACTIONS IN STARS: PRINCIPLES OF STELLAR EVOLUTION AND NUCLEOSYNTHESIS

Nonresonant reactions: also known as direct reactions; occur without the formation of an intermediate compound nucleus

Resonant reactions: can be regarded as a two-step process and often proceed through an excited state of the compound nucleus

Broadly speaking, quiescent (i.e., nonexplosive) stellar evolution proceeds through a sequence of gravitational contractions and distinct stages of nuclear fusion during which new chemical elements are produced. Stars form from molecular gas clouds composed of ^{1}H and ^{4}He (75% and 25% by mass, respectively) and traces of heavier elements. As the gas cloud collapses, about half of its gravitational energy is radiated away while the other half is converted into heat, thus increasing the gas temperature. Provided the mass of the protostellar cloud is large enough, sufficiently high temperatures ($T \sim 10^{6}$–10^{7} K) can be reached in the star's innermost regions to trigger nuclear fusion reactions. These liberate energy and stabilize the star against further gravitational contraction. What happens next critically depends on the initial mass of the collapsing cloud and, to a lesser extent, its initial chemical composition.

The first, and longest, of the nuclear burning epochs, hydrogen burning, converts hydrogen into helium over typical timescales from 10^{10} y for a star like our Sun to only 10^{6} y for a star of about 40 solar masses ($M_{\odot}$). After all hydrogen in the core has been exhausted, the star can no longer support the weight of its outer layers, and gravitational contraction sets in once again, further heating the stellar core. Low-mass stars like the Sun will experience helium burning, producing carbon and oxygen through the fusion of ^{4}He nuclei (α particles) via the so-called 3α process ($3\alpha \rightarrow {}^{12}\mathrm{C} + \gamma$) and the $^{12}\mathrm{C}(\alpha,\gamma)^{16}\mathrm{O}$ reactions. Low-mass stars will eventually die as white dwarfs, i.e., highly dense and compact objects supported by electron degeneracy (5). By contrast, more massive stars ($M > 8M_{\odot}$) will evolve through more advanced stages of nuclear fusion (carbon-, neon-, oxygen-, and silicon-burning), each leading to the synthesis of increasingly heavier elements up to Fe, before finally exploding as core-collapse supernovae.

In a stellar plasma, nuclear reactions are initiated by the thermal motion of nuclei and are therefore referred to as thermonuclear reactions. For a nonrelativistic and nondegenerate plasma in thermodynamic equilibrium at a temperature T, the relative velocity distribution of nuclei is well described by the Maxwell–Boltzmann distribution, $\phi(v)\mathrm{d}v = \phi(E)\mathrm{d}E \propto \sqrt{E}\exp(-E/kT)$, where $k = 8.6173 \times 10^{-5}$ eV/K is the Boltzmann constant. However, the energy kT, at which the velocity distribution reaches its maximum, turns out to be always smaller than the repulsive Coulomb barrier between the interacting nuclei. For example, at temperatures $T \simeq 15 \times 10^{6}$ K (as in the center of the Sun), the average energy of the ions in the plasma is $kT \simeq 1.3$ keV, i.e., much lower than the Coulomb repulsion between even the lightest of charges, namely two protons ($E_{\mathrm{Coul}} = 0.5$ MeV). It follows that nuclear reactions in stars are only possible thanks to the quantum-mechanical tunneling through the Coulomb barrier. In the absence of a centrifugal barrier that would further hinder a fusion reaction, the tunneling probability can be described by an exponentially decreasing function of energy as $\exp(-2\pi\eta)$, with $2\pi\eta = 31.29\, Z_1 Z_2 (\mu/E)^{1/2}$ [Z_i being the atomic numbers of the interacting particles, μ their reduced mass in atomic mass units, and E the center-of-mass energy in keV (5)].

The cross section $\sigma(E)$ for a nonresonant reaction can then be expressed as

$$\sigma(E) = \frac{1}{E}\exp(-2\pi\eta)\, S(E), \qquad 1.$$

where $1/E \propto \pi\hbar^{2}$ is a non-nuclear term involving the de Broglie wavelength of the interacting nuclei, and the astrophysical $S(E)$ factor, defined by this equation, contains all the strictly nuclear physics effects of the interaction. Note that for nonresonant reactions, the astrophysical $S(E)$ factor varies little with energy.

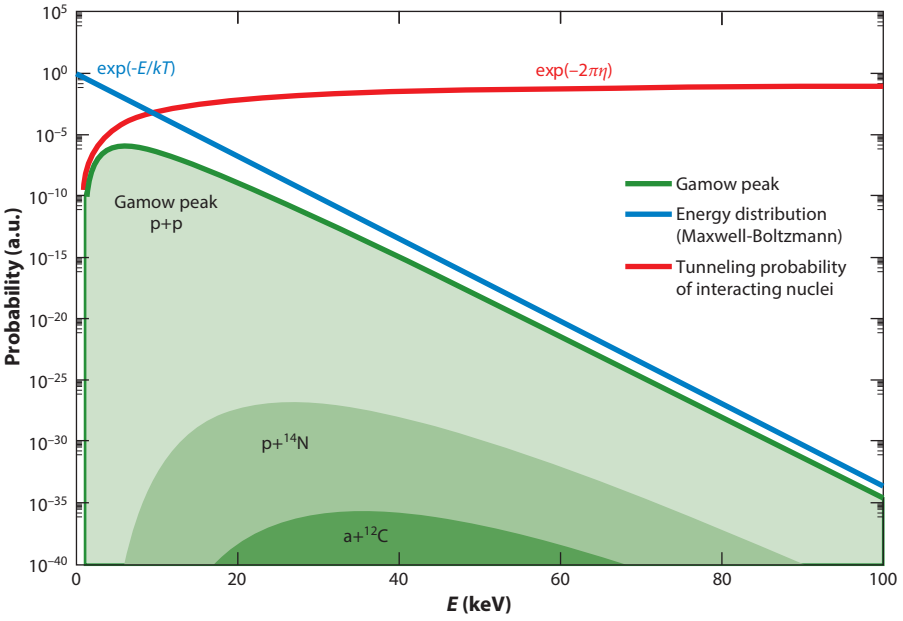

Figure 1

The Gamow peak curve (*green*) arises from the product of the Maxwell–Boltzmann distribution (*blue*) at a temperature T (here $T = 15 \times 10^6$ K) and the tunneling probability (*red*) between the interacting nuclei. The integral of the peak (*shaded area*) is proportional to the reaction rate. Note how, at the same temperature, the Gamow peak curves shift to higher energies for reactions between higher-Z nuclei and become progressively smaller because of the correspondingly lower tunneling probabilities (shown here only for the p+p case). Abbreviation: a.u., arbitrary units.

The key quantity of interest for astrophysical purposes is not just the cross section, but the reaction rate per particle pair, defined as follows:

$$\langle \sigma v \rangle = \int_0^\infty \phi(v)\, v\, \sigma(v)\, \mathrm{d}v = \int_0^\infty \phi(E)\, v\, \sigma(E)\, \mathrm{d}E \propto \int_0^\infty S(E) \exp\left[-E/kT - 2\pi\eta\right] \mathrm{d}E, \quad 2.$$

with v being the relative velocity between the interacting particles. The product of the Maxwell–Boltzmann distribution and the tunneling probability gives rise to a peak-shaped curve, commonly referred to as the Gamow peak (as shown in **Figure 1**), which represents the energy region at which a given reaction is most likely to occur or, equivalently, the energy region that maximizes the reaction rate per particle pair. To a first approximation, the reaction rate $\langle \sigma v \rangle$ is proportional to the area under the Gamow peak (see Reference 5 for a more detailed and rigorous account of this derivation), and at any given temperature, its value drops dramatically by several orders of magnitude as the charges of the interacting particles increase (**Table 1**). Incidentally, this explains why stellar evolution proceeds through well-defined stages of nuclear burning: Nuclear reactions involving heavier and heavier elements require ever increasing temperatures, which can only be attained through the gravitational contraction that follows the exhaustion of a previous nuclear fuel in the core of the star.

As the star evolves, its temperature changes, and so will the location and width of the Gamow peak of a given reaction as well as the associated astrophysical reaction rate $\langle \sigma v \rangle$ (**Figure 1**). Stellar models and nucleosynthesis network calculations therefore require the accurate knowledge of hundreds of nuclear reaction cross sections, each over a broad energy region. Unfortunately,

Table 1 Coulomb barriers and Gamow peak energies for nuclear reactions between nuclei with increasing charge numbers, at a temperature $T = 15 \times 10^6$ K

Reaction	Coulomb barrier	Gamow peak	Peak integral $\propto \langle \sigma v \rangle$
p + p	0.55 MeV	5.9 keV	1.1×10^{-6}
p + ^{14}N	2.27 MeV	6.8 keV	1.8×10^{-27}
α + ^{12}C	3.43 MeV	56 keV	3.0×10^{-57}
^{16}O + ^{16}O	14.07 MeV	237 keV	6.2×10^{-239}

The last column represents the area under the Gamow peak, a proxy for the corresponding nuclear reaction rates (see text and Reference 5 for details).

because of our limited knowledge of nuclear forces and interactions, it is difficult to accurately predict nuclear reaction cross sections as a function of energy from first principles. Instead, these must be determined experimentally. In the next section we explore the main challenges and the key requirements for laboratory measurements of reactions between stable nuclei at the energies of astrophysical interest.

3. NUCLEAR REACTIONS IN THE LABORATORY: CHALLENGES AND REQUIREMENTS

Nuclear reactions of astrophysical interest can be studied in the laboratory using a particle accelerator capable of delivering a beam of ions (often protons or α particles) onto a suitable gas or solid-state target over a broad energy range. The target is surrounded by detectors sensitive to the type of radiation (i.e., γ-rays, charged particles, or neutrons) produced by the reaction under study. Ideally, reaction cross sections should be measured directly at the Gamow peak for the given pair of interacting nuclei and at the relevant stellar temperature. Sadly, this is easier said than done. Because of the steep exponential drop associated with the tunneling probability (Equation 1), cross sections are typically in the pico- to femtobarn range (1b $= 10^{-24}$ cm^2) and translate into extremely low counting rates, ranging from a few counts per hour to a few counts per year in the most extreme cases. Therefore, cross section evaluations at stellar temperatures often rely on extrapolations from data taken at higher energies. While such extrapolations are often performed with the aid of theoretical formalisms, such as the *R*-matrix (6), uncertainties often remain because of possible contributions from unknown resonances (either above or below threshold) and because of the unclear influence of the electron screening effect (7) at the lowest interaction energies.

To guide cross section extrapolations, significant effort must be devoted to pushing direct measurements to lower and lower energies, which poses considerable challenges and requires a number of expedients to increase the signal-to-noise ratio of the reaction under study. Improvements are generally achieved by a combination of measures aimed at increasing the signal (e.g., through maximizing beam currents, target density, and detection efficiencies) and reducing the noise (i.e., the background signal), both natural and beam induced. These measures are discussed in the following sections, together with a few additional requirements not normally encountered in ordinary nuclear physics experiments.

3.1. Long-Term Stability of Accelerators and Targets

The low cross sections of astrophysical reactions necessitate high beam intensities and long irradiation times of up to several months. The long-term stability of both accelerators and targets is thus crucial. Modern accelerators provide good energy stability over time, but dedicated tests

are often required for nuclear astrophysics applications. Highly automatized systems allowing for unattended, remote operation are also useful but require reliable safety solutions.

Long irradiation times at high beam currents may easily result in strong target degradation in the case of solid-state targets. Sputtering of the target material, heat-induced effects, and implantation of the beam particles may alter the target properties. Thus, the choice of the target material and the preparation method must be optimized for target stability, and target degradation must be kept under control. Before the actual cross section measurements, fresh targets are usually characterized through suitable ion beam analysis methods (8) to accurately determine their thickness, composition, and stoichiometry (in case of compounds). Repeated measurements of these target properties in the course of the experiment are used to monitor the target degradation and keep it at an acceptable level (9). Depending on the precision required for the cross section measurement, some degree of degradation—if precisely known—may be tolerated, but the replacement of spent targets with fresh ones is eventually needed after a certain amount of charge has been accumulated.

3.2. Accurate Knowledge of Interaction Energy

In addition to the energy stability (in time) of the ion beam, precise knowledge of its absolute energy and energy spread are also necessary at sub-Coulomb energies because the steep energy dependence of nonresonant cross sections sensitively affects the stellar reaction rate $\langle \sigma v \rangle$. For example, in the ^{3}He(α,γ)^{7}Be reaction, a 1-keV beam energy uncertainty at $E_\alpha = 220$ keV (a 0.5% error) translates into a 4% uncertainty in the cross section. Similarly, the rate of reactions dominated by narrow resonances depends exponentially on the energy of the resonant state (5). Thus, a precise energy calibration of the accelerator beam energy must be carried out. This is typically achieved by exploiting suitable nuclear reactions that exhibit resonances of very well-known energy. Depending on the dynamic range of the accelerator, different reactions may be exploited. For example, the ^{23}Na(p,γ)^{24}Mg, ^{25}Mg(p,γ)^{26}Al, and ^{26}Mg(p,γ)^{27}Al reactions have all been used below 400 keV to a precision of $\pm$300 eV (10). Higher-energy accelerators can make use of neutron threshold reactions (11) or other well-known resonances, e.g., in the ^{27}Al(p,γ)^{28}Si reaction.

The accurate knowledge of interaction energy poses requirements not only on the accelerator itself but also on the target properties. As the beam loses energy when traversing the target, the cross section is effectively measured over a finite energy range rather than at a single energy. Information about the target thickness and composition is thus needed in order to calculate the effective energy of the measured cross section. This holds for both solid-state and gas targets. For gas targets, the so-called beam heating effect (i.e., the increase in gas temperature due to the power deposited by the beam) further complicates the energy loss determination and needs to be carefully studied (12). Extended gas targets often have physical dimensions larger than the size of typical detectors. Since the detection efficiency may depend strongly on the position at which the nuclear reaction occurs, the energy loss of the beam in the target gas must be convoluted with the detector efficiency in order to determine the effective interaction energy and its associated cross section (13).

3.3. Detectors

Requirements for the detection setup include a high efficiency and sensitivity to the radiation produced by the reaction under study, and—at the same time—a high signal-to-background ratio. This condition can be achieved either by reducing backgrounds seen in the detector (as discussed below) or by optimizing the detected signal, e.g., through improved energy resolution, the use of pulse-shape discrimination, or the use of detectors with independent sensitive volumes to allow

for powerful coincidence or anticoincidence configurations. Once again, the long data-taking times of low-yield experiments call for a long-term stability of the detection apparatus and related electronics, so frequent calibration measurements are needed to periodically check the detector response. This is particularly true for low background experiments where low statistics prevent identification of the region of interest from the measurement itself.

3.4. Backgrounds

So far, we have looked at ways to maximize the counting rate by improving the signal through increased beam intensity and detection efficiency. However, the most insidious limitation to nuclear astrophysics experiments often arises from background signals that can mimic the signature of the reaction of interest but are, in fact, caused by different processes and therefore limit the sensitivity of the experiment. Techniques to mitigate the various sources of background are highly specific to the type and origin of the background and typically include material screening, surface cleaning, active or passive shielding, and the rejection of background signals by pulse-shape discrimination techniques (14).

Background sources can be grouped according to their origin as follows: beam induced, intrinsic, and environmental. In accelerator-based experiments, beam-induced backgrounds originate from spurious interactions of the ion beam with the experimental setup. These may occur in the target material, or at any other point along the path of the beam. Reactions on trace contaminants in the target material (often light elements with low Coulomb barriers) can be reduced by choosing chemically pure materials for target production, by treating these materials through etching to reduce surface contaminants (15, 16), or by heating the targets to drive out contaminants from their bulk (17). Similar considerations apply to other components along the beam path (e.g., apertures or collimators), which should typically be chosen to have a large atomic number (e.g., tungsten) and be frequently cleaned. For solid targets, careful handling and storage (e.g., under protective atmosphere to avoid oxidation or absorption of humidity) may reduce the risk of target contamination in the time between target production and measurement.

Intrinsic backgrounds are present in the experimental setup, most critically in the detection material itself. Radioactive nuclides in the detector medium may cause background signals through the emission of radiation in their decay. These radioactive nuclides may be part of a decay chain originating from long-lived primordial nuclides. Nuclides with shorter lifetimes may arise from artificial radioactivity (i.e., produced in man-made processes) or cosmogenic activation (i.e., produced through interactions with cosmic rays). For geometrical reasons, the closer this radiation is to the sensitive volume of the detector, the more likely it is to result in a background signal. This is especially true for charged particle radiation because of its short range in matter.

Finally, environmental (i.e., ambient) backgrounds are caused by the radiation field at the location of the experiment, which is present independently of the experimental setup. This includes natural radioactivity, as well as the effects produced by cosmic radiation. These sources of environmental radiation may result in background signals through their direct interaction with the detector setup. For example, characteristic γ-ray energies from the decay of radionuclides in the long-lived decay chains are readily observed in a high-resolution γ-ray detector. Environmental radiation may also contribute to the detector background through secondary effects, such as (α,n) reactions induced by the α particles produced in a radioactive decay and leading to secondary neutrons. Environmental γ-ray background is often reduced by shielding the detection setup with active and/or passive high-purity and high-Z materials (typically lead and copper). Yet, the best and most effective way of reducing a major source of natural background is to perform experiments deep underground, where the influence of cosmic rays can be greatly reduced. The

validity of this approach was dramatically demonstrated with the installation of a small accelerator specifically designed for nuclear astrophysics studies.

In the following section, we describe how the many requirements presented here have been successfully met at the Laboratory for Underground Nuclear Astrophysics (LUNA), the first laboratory of its kind worldwide. After summarizing LUNA's components and instrumentation, we show how the underground location has proved instrumental for studying not just reactions producing γ-rays but also those emitting charged particles or neutrons.

4. NUCLEAR ASTROPHYSICS UNDERGROUND: THE LUNA FACILITY

4.1. Accelerators

LUNA was established in 1991 with the installation of a 50-kV accelerator at the LNGS (Laboratori Nazionali del Gran Sasso) of the Italian INFN (Istituto Nazionale di Fisica Nucleare). The accelerator was specifically designed to investigate nuclear reactions from the p–p chain at energies close to the solar Gamow window[2] (19). Thanks to the success of those early measurements (see Section 5), the pilot accelerator was replaced in 2001 with a 400-kV electrostatic machine, which is still in operation today (10). Its energy range has allowed for the investigation of many key reactions at the relevant energies of hydrogen burning in different phases of stellar evolution, including during the main sequence, the red giant branch and asymptotic giant branch (AGB) stages, classical novae explosions, and big bang nucleosynthesis (BBN) (see Section 5 for key scientific highlights).

In the LUNA 400-kV accelerator, the high voltage is produced by an inline Cockcroft–Walton power supply capable of handling currents as high as 1 mA at 400 kV (10). A radio-frequency source provides 1 mA H^+ beams and 500 μA He^+ beams. Once extracted, the beam is accelerated and redirected by 45° magnets, either toward the gas- or toward the solid-target station. The absolute beam energy is calibrated to a precision of ±300 eV, the proton energy spread is lower than 100 eV, and the long-term energy stability is 5 eV h^{-1} (10). In addition, a number of safety interlocks allow the machine to operate in stable conditions, even without human supervision. These characteristics make LUNA 400-kV the ideal machine for nuclear astrophysics experiments requiring long data-taking periods.

4.2. Beam Lines: Solid and Gas Target Stations

The LUNA 400-kV accelerator is equipped with two beam lines: one hosting a windowless gas target system and the other hosting a solid target station, as shown in **Figure 2**. Thanks to the two setups, it is possible to work with a wide range of target materials. Also, some nuclear reactions can be studied independently both with the gas target and with solid targets, to check for possible systematic effects due to target properties. As mentioned in Section 3, gas targets have the advantage of being stable upon irradiation with intense ion beams but require complex pumping systems, more elaborate techniques to determine the beam current, and precise density profile measurements. In contrast, solid targets are comparatively easier to handle, but they need to be periodically checked for degradation due to beam irradiation.

The LUNA windowless gas target system consists of three differential pumping stages. The absence of windows to confine the gas preserves the beam energy distribution before it enters the

[2]By approximating the Gamow peak curve to a Gaussian function, the Gamow window can be defined as the $1/e$ width Δ of the Gaussian function. The Gamow window therefore represents the energy region that makes the most contribution to the area under the Gamow peak (see Reference 18 for a rigorous derivation).

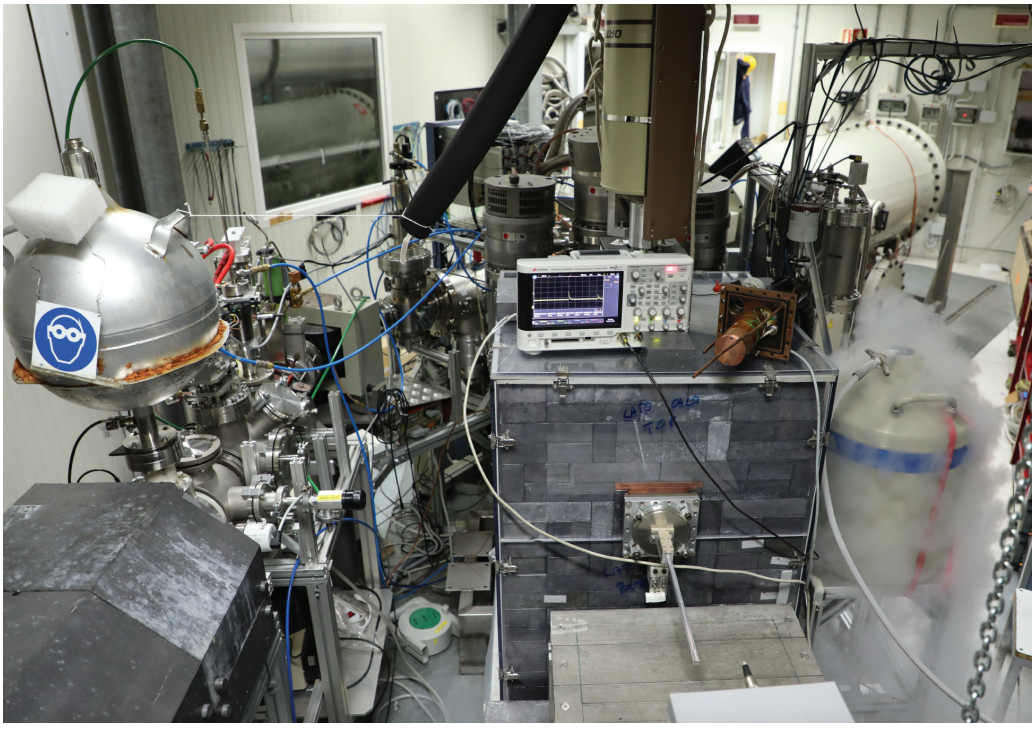

Figure 2

Picture of the LUNA 400-kV accelerator (*background*, *top right*) and the two beam lines (*foreground*). Both the solid target (*left*) and gas target (*center*) setups are surrounded by massive lead shields for further background suppression.

target chamber. A continuous gas flux adjusted by a feedback system maintains a constant pressure in the range of 0.1–10 mbar inside the target chamber. The gas is continuously pumped from the chamber through three pumping stages that gradually bring the pressure down to the 10^{-7}-mbar range. The pumping stages are separated by long, water-cooled apertures of decreasing diameter that serve both to collimate the beam and to increase the impedance for the gas flow from the target to the pumping stages. The gas taken from the pumping stages can be either discharged or collected, purified, and recirculated back into the gas target. Inside the target chamber, the beam is stopped on a beam calorimeter providing continuous and accurate beam current measurements. The target chamber geometries can be adapted to couple the gas target with different types of detectors.

The second beam line ends with a solid target station. Different vacuum chambers have been designed over the years to meet the requirements of individual experiments. In general, the target backings used are characterized by high purity levels and are thick enough to stop the beam. The target backing is therefore directly water cooled to dissipate the power deposited by the beam. To reduce contaminant deposition on target, the vacuum chamber is equipped with a copper pipe cooled to liquid nitrogen temperature. The pipe is electrically insulated from the chamber and biased to typical voltages of −300 V to suppress secondary electrons produced when the beam hits the target. The chamber and target holder are electrically insulated from the beam line and, in this configuration, act as a Faraday cup for beam current integration.

4.3. Detectors

Various detectors have been used at LUNA, each with a dedicated target chamber. For the detection of γ-rays, high-resolution spectroscopy is performed with large-volume, high-purity germanium (HPGe) detectors. All LUNA HPGe detectors are made from materials with low intrinsic background to preserve the advantages of being underground. Over the years, different target-detector geometries have been adopted, depending on the requirements of the reaction under study. In addition, when γ-rays with energies lower than 3 MeV need to be detected, thick passive shielding made of lead and copper is used to suppress the environmental background due to naturally occurring radioactive isotopes (see also Section 4.4). If extremely weak cross sections are to be measured and the sensitivity needs to be pushed to the limit, a large-volume bismuth germanate (BGO) detector covering almost the full solid angle around the target is used. The detector is optically segmented into six sections, with each crystal coupled to a photomultiplier. The BGO detector has low energy resolution but can be used as a calorimeter by summing the energies of all coincident γ-rays detected in any of its sections. With this approach, only one peak is observed in the spectrum at the nuclear excitation energy, and the detection efficiency can be up to 60% in some cases. Lately, the BGO detector has also been used successfully to determine γ-decay branching ratios exploiting γ-γ coincidences in sections pairs.

More recently, the LUNA collaboration has expanded its detector suite with the addition of an array of large area silicon detectors for charged particle detection (Section 4.4.2) and a set of ^{3}He counters for neutron detection (Section 4.4.3).

4.4. Background Suppression Deep Underground

In the following, we present three examples of recent studies that demonstrate how going underground has been instrumental not just for the detection of γ-rays but also for the detection of charged particles and neutrons.

4.4.1. γ-Ray detection: the ^{2}H(p,γ)^{3}He reaction. The study of nuclear reactions emitting γ-rays is especially favorable underground because of the natural background suppression afforded by the rock overburden. The 1.4 km (3,800 meters of water equivalent, m.w.e.) of rock above LNGS, for example, leads to a six-order-of-magnitude suppression of the cosmic-induced background at γ-ray energies above 3 MeV, as shown in **Figure 3*a***. At lower energies, the γ-ray background is dominated by γ-rays emitted in the decay of naturally occurring radioactive isotopes. However, in this energy region, a deep underground location brings a substantial advantage. This component of the γ-ray background is typically suppressed by surrounding the detector with passive shielding made of high-purity and high-Z materials (typically lead and copper). On the Earth's surface, the thickness of the shielding is limited by the fact that the interaction of cosmic rays within the shielding itself produces radioactive isotopes and secondary radiation. This problem is significantly reduced underground, where a much thicker shielding can then be used.

As an outstanding example of the potential of underground experiments aimed at detecting γ-rays, we present the case of the ^{2}H(p,γ)^{3}He reaction ($Q = 5.5$ MeV). This reaction plays a key role in the first minutes of the life of the Universe, as it contributes to deuterium destruction during BBN. In BBN studies, deuterium abundance is used as an indicator of cosmological parameters since it is particularly sensitive to the baryon density, or alternatively the baryon-to-photon ratio, of the early Universe. Until recently, however, the ^{2}H(p,γ)^{3}He cross section represented the main source of uncertainty on the predicted abundance of primordial deuterium (21). The uncertainty was due to the lack of experimental data at the energies of interest for BBN (30–300 keV), where only two data sets were available in the literature (22, 23), both with relatively high systematic

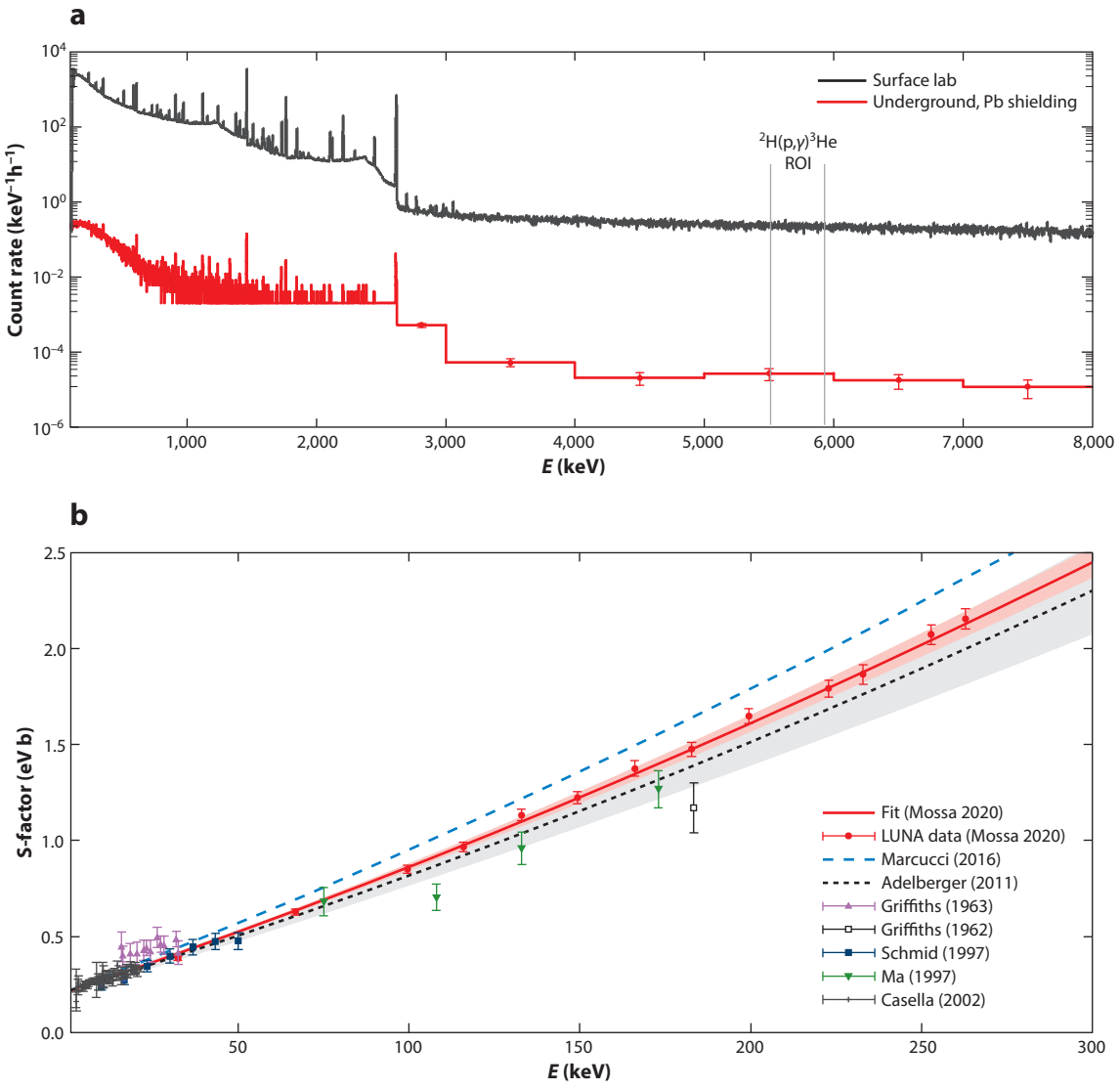

Figure 3

(*a*) Background spectra recorded with a HPGe detector on the Earth's surface (*black*) and underground at LUNA (*red*), with the copper and lead shielding described in Reference 20. Vertical lines define the ROI for the γ-rays expected from the ^{2}H(p,γ)^{3}He reaction. (*b*) Astrophysical S-factor of the ^{2}H(p,γ)^{3}He reaction. The LUNA results are compared with the literature. Abbreviations: HPGe, high-purity germanium; ROI, region of interest. Figure adapted with permission from Reference 26.

errors. The ^{2}H(p,γ)^{3}He cross section was also evaluated by ab-initio calculations (24), but the difference between theoretical calculations and experimental data led to some ambiguity in the choice of the cross section for BBN models and resulted in a high uncertainty on the inferred cosmological parameters (21).

At LUNA, the ^{2}H(p,γ)^{3}He reaction was studied at center-of-mass energies between 30 and 263 keV using the windowless gas target system and an HPGe detector mounted in close geometry (25). The reaction cross section was measured with an unprecedented low systematic error ($\lesssim$3%)

(26) (see **Figure 3*b***). These results allowed us to significantly reduce the uncertainty on BBN predictions of the baryon density and the effective number of neutrino families (26). Thanks to the new LUNA data, the cosmological parameters provided by BBN models are now in better agreement with those derived from the analysis of the cosmic microwave background anisotropies, thus supporting the standard cosmological model (26).

AGB stars: stars with higher luminosities but lower surface temperatures than the Sun; their name arises from their position in the Hertzsprung–Russell diagram

4.4.2. Charged-particle detection: the ^{17,18}O(p,α)^{14,15}N reactions. In a silicon semiconductor, the energy spectrum of cosmic muons shows a maximum near zero and decreases exponentially with energy (27). As cosmic muons are significantly suppressed underground, one can expect improved signal-to-background ratios in deep-underground experiments aimed at detecting charged particles with silicon detectors. Indeed, improved background suppression was demonstrated in the study of the ^{17,18}O(p,α)^{14,15}N reactions (28, 29), which play an important role in the nucleosynthesis of key isotopes used to constrain stellar models of novae, AGB, and post-AGB stars. Both reactions were studied at LUNA using an intense proton beam onto solid Ta_2O_5 targets enriched in either ^{17}O or ^{18}O. The main goals were to measure (*a*) the strength of the $E_p = 70$ keV resonance in the ^{17}O(p,α)^{14}N reaction and (*b*) the excitation function of the ^{18}O(p,α)^{15}N reaction at energies $E_p = 60$–360 keV, to determine the strengths of four resonances of astrophysical interest. Because of the low beam energies required, the kinematics of the emitted α particles were essentially governed by the Q-values of the ^{17}O(p,α)^{14}N and ^{18}O(p,α)^{15}N reactions (1.192 and 3.98 MeV, respectively).

Thus, a purpose-built scattering chamber was developed to detect low-energy ($E_\alpha \simeq 200$ keV and 2.3 MeV, respectively) α particles with maximum efficiency. The setup consisted of an array of six passivated implanted planar silicon detectors (with thickness 300-700 μm and active area 9 cm^2) arranged over two rows at angles of 135.0° and 102.5°, with an overall efficiency of 15% (30). Each detector was protected by aluminized mylar foils of appropriate thickness, carefully chosen to suppress the large flux of elastically scattered protons while allowing for the passage of the α particles with minimal energy loss.

In order to quantify the background reduction underground, measurements were performed both overground (in Edinburgh, United Kingdom) and underground (at LUNA) using the same setup and electronics, both with and without a shield of lead bricks arranged around three sides of the chamber. The results (30) are shown in **Figure 4**. At energies up to about 1.5 MeV, the spectra are dominated by a long exponential tail that is suppressed by a factor of about 15 for the underground shielded setup compared with the overground unshielded measurement.

The strongest background suppression (a factor of ∼23) is observed around 2,000 keV, before gradually reducing to a factor of ≃2 at 4,000 keV. In the energy region $E \simeq 2{,}000$-$4{,}000$ keV, the lead shielding does not appear to have a major effect either overground or underground. Although the source of background in this region is not obvious, we note that the contribution from the low-energy tail of the broad peak at $E \simeq 5{,}500$ keV is especially important underground. This broad peak is likely due to the intrinsic activity of the silicon detectors since its contribution is not affected by either the lead shielding or the underground environment.

The combined effects of the background suppression underground and the generally improved experimental conditions (30) have led to the most accurate value to date for the $E_p = 70$ keV resonance strength $\omega\gamma$ in ^{17}O(p,α)^{14}N, namely $\omega\gamma = (10.0 \pm 1.4_{stat} \pm 0.7_{syst})$ neV. In turn, this has led to a factor-of-two increase in the ^{17}O(p,α)^{14}N reaction rate and to a reduced ^{17}O/^{16}O ratio, with important consequences for the origin of some oxygen-rich group II presolar grains (31). Similarly, we have obtained improved results on the ^{18}O(p,α)^{15}N cross sections and resonance strengths, with tighter constraints on oxygen isotopic ratios (29). Future (p,α) measurements are expected at the LUNA 400-kV accelerator in the next three-year scientific program (2022–2024).

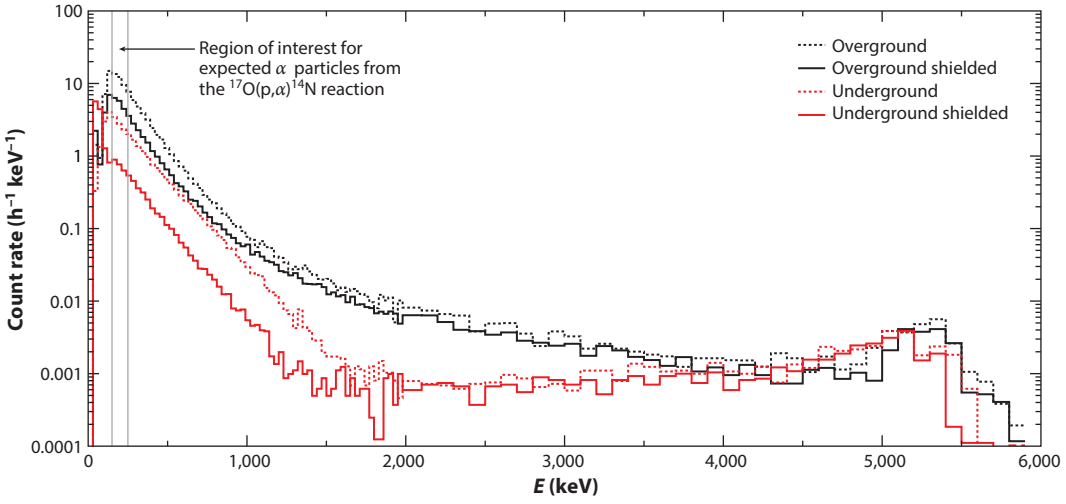

Figure 4

Background spectra obtained with passivated implanted silicon detectors overground (*black lines*) and underground (*red lines*) with (*solid*) and without (*dashed*) lead shielding (30). The vertical lines indicate the region of interest for the detection of low-energy α particles from the $^{17}O(p,\alpha)^{14}N$ reaction. Figure adapted with permission from Reference 30.

4.4.3. Neutron detection: the $^{13}C(\alpha,n)^{16}O$ reaction. In a deep underground environment, the neutron background is mainly created by fission and (α,n) reactions as a result of natural radioactivity in the surrounding material. The production of neutrons by cosmic rays, while dominant in surface and shallow underground laboratories (32), is largely suppressed deep underground, thanks to the reduction of cosmic rays by the rocks overhead. Neutron flux measurements have been performed in different underground locations, with different detection techniques and capabilities, to obtain information on the neutron energy spectrum (33–35). The difference in neutron flux on the Earth's surface and deep underground can be several orders of magnitude [about 3 for thermal neutrons at LNGS (36)].

The sensitivity of a detector setup to the neutron background flux is closely related to the detection technique. While detectors based on neutron capture reactions, such as ^{3}He counters, are primarily sensitive to thermalized neutrons, organic scintillators based on elastic neutron scattering on hydrogen are only sensitive to neutrons above a threshold energy. The addition of materials (mostly hydrogen rich) as neutron shielding around the detection setup may be used to alter the neutron energy spectrum (i.e., to thermalize the neutrons) or to reduce the neutron flux through neutron capture reactions [e.g., $^{1}H(n,\gamma)$, $^{10}B(n,\alpha)$, or $^{6}Li(n,\alpha)$].

These efforts can reduce backgrounds induced by environmental neutrons, but backgrounds intrinsic to the detectors should also be considered, as they can eventually become the limiting factor. In particular, α backgrounds may closely resemble the neutron signal. Material screening and selection for low intrinsic radioactivity may be required. Depending on the detection principle that is employed, pulse-shape discrimination may offer further improvements.

As a specific example, we describe the detection setup for a recent study of the $^{13}C(\alpha,n)^{16}O$ reaction, a main source of neutrons for the s-process. The reaction cross section was measured at LUNA (36–38) using an array of 18 stainless steel ^{3}He counters to detect the neutrons produced during the bombardment of ^{13}C targets with a $^{4}He^{+}$ beam. The counters were embedded in a high-density polyethylene moderator to thermalize the neutrons and arranged in two concentric rings around the target chamber: The inner radius contained six counters of 25 cm

active length, while the outer radius hosted 12 counters of 40 cm active length. This configuration allowed for a nearly 4π solid angle coverage around the target, with an overall detection efficiency on the order of 40% (36). The configuration of the moderator and counters was chosen to optimize the sensitivity to the neutrons produced by the $^{13}C(\alpha,n)^{16}O$ reaction (Q-value = 2.216 MeV). Outer layers of borated polyethylene (with a boron content of 5% by weight) were added to capture environmental neutrons and reduce their background contribution to the spectrum.

Figure 5*a* illustrates the effects of the underground location on the neutron background spectrum, as well as the importance of an appropriate choice of materials. The use of a stainless steel housing provides a dramatic reduction of the intrinsic α background compared with prior tests using counters with an aluminum housing (34). The two spectra acquired underground with counters made from materials of different radiopurity underline the influence of material selection on the sensitivity of the detection setup. In addition, pulse-shape discrimination helped to reduce background events caused by the remaining α activity in the walls of the detector (38).

The combination of these techniques has allowed, for the first time, background reduction to the level required to extend the measurement of the $^{13}C(\alpha,n)^{16}O$ cross section down to the Gamow window (37). The results from this measurement at LUNA are shown in comparison with other data from the literature in **Figure 5*b*** and highlight the role of these low-energy data points in constraining the fit. In this energy region, the experiment is approaching a regime where the experimental yield is the limiting factor, rather than the background level. Measurements with high beam intensity at JUNA (see Section 6.2) aim to overcome this limitation and reach even lower energies. Future measurements over a wider energy range, at JUNA with He^{++} or at LUNA MV (Section 5.6), are expected to help in solving discrepancies in the normalization of different literature data sets and thus reduce the systematic uncertainty on the cross section of this important reaction.

4.5. Activation Experiments and Low Background Counting

The reaction cross section measurements discussed so far are based on the detection of the radiation (γ-rays, charged particles, or neutrons) emitted by the reaction under study. A completely different method to measure reaction cross sections is based on the activation of the irradiated target (41). Here the number of reactions is determined from the measurement of the radioactive decay of the reaction product. The technique involves two phases: First, a target is irradiated with an ion beam, and second, the decay of the produced isotope is measured. The obvious limitation of the activation method is that the reaction product must be radioactive—reactions leading to stable isotopes cannot be investigated. In addition, the half-life of the residual nucleus must be suitable, and the decay must be followed by the emission of some kind of radiation that can be detected. Usually, γ radiation is preferred, as it allows for the identification of the decaying isotope.

If the basic requirements are fulfilled, the activation method has some advantages compared with the conventional in-beam techniques. The radiation from a radioactive decay is isotropic, and thus there is no need to care about angular distribution effects. There is no risk of missing some of the yield by nondetected weak transitions. The background is usually much lower because no prompt beam-induced background needs to be considered. Since the number of reactions is determined from the decay, the total cross section is obtained directly, which is the astrophysical quantity of interest for the reaction rate calculation. However, the different transitions contributing to the production of the residual nucleus are not measured, and hence no spectroscopic information is gained that could be used, for example, in R-matrix fits. In many cases the activation method can be a useful alternative approach to the cross section measurement carried out with

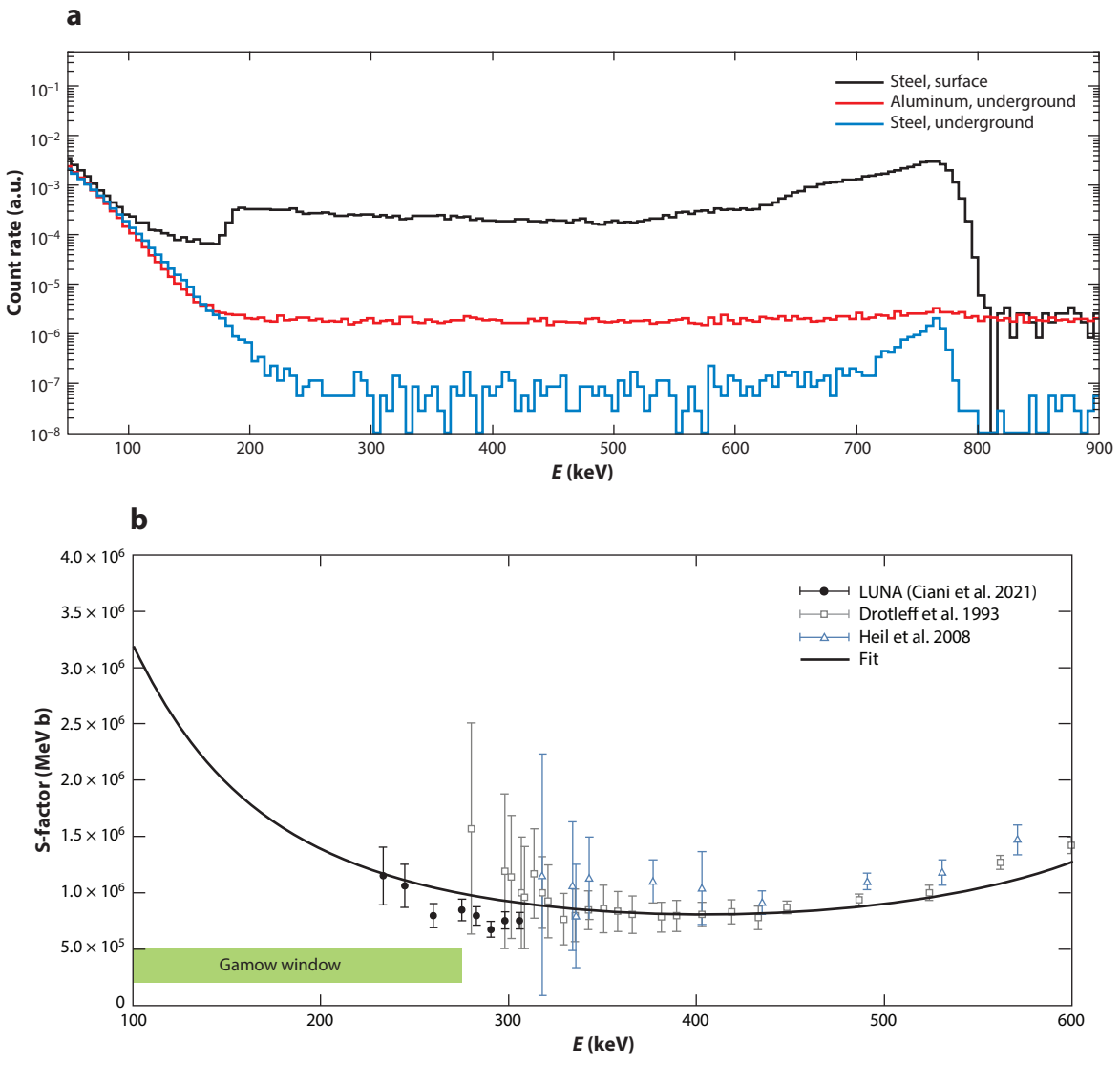

Figure 5

(*a*) Qualitative comparison between background spectra for thermalized neutrons (leading to the peak at 764 keV) as obtained with ^{3}He counters of different sizes and materials, overground (*black*) and underground (*red* and *blue*). Note how the low levels of intrinsic radioactivity of the stainless steel housing afford a further background reduction underground compared with traditional aluminum counters. (*b*) Astrophysical S-factor of the $^{13}C(\alpha,n)^{16}O$ reaction. The high precision of the LUNA data (*solid symbols*) (37), for the first time within the Gamow window (*green shaded area*), places stronger constraints on the theoretical fit (*black line*). Previous literature data are taken from References 39 and 40. Abbreviation: a.u., arbitrary units. Figure adapted with permission from Reference 36.

in-beam spectroscopy, and thus, a comparison of the results from the two techniques can be used to identify possible systematic uncertainties. The combination of the two methods can lead to improved accuracy of the final results.

4.5.1. Underground studies. In the following, we provide some examples of activation experiments in underground laboratories. The first group of reactions was studied by the LUNA

collaboration, and both the irradiation and the decay counting were done underground at LNGS. In a second group of reactions, the activation was performed at accelerators on surface laboratories, and only the decay counting was carried out in a deep underground environment. Finally, we describe a case where accelerator mass spectrometry was exploited.

4.5.1.1. $^{3}He(\alpha,\gamma)^{7}Be$. This reaction is one of the key reactions of the p–p chains of solar hydrogen burning (42). ^{7}Be decays by electron capture to ^{7}Li with a half-life of 53.22 days, and the decay is followed by the emission of a 478-keV γ-ray. LUNA has measured the cross section of this reaction by both in-beam γ spectroscopy and activation method. Prior to this measurement, there was an apparent discrepancy between the results obtained with the two methods for this reaction. This fact significantly increased the uncertainty of the cross section, which made this one of the least-understood reactions of hydrogen burning. The high-precision LUNA results obtained with the two methods were in excellent agreement and significantly reduced the overall uncertainty budget of this reaction (43–45).

4.5.1.2. $^{17}O(p,\gamma)^{18}F$. This reaction takes place in explosive hydrogen burning processes such as, for example, classical novae. The half-life of the reaction product (109.77 min) is much shorter than that of ^{7}Be but still long enough that, after the irradiation, the target can be removed from the reaction chamber and transported to a low background counting setup using a shielded HPGe detector. ^{18}F decays by positron emission, and the decay is not followed by γ emission. The detection of the 511 keV positron annihilation radiation, however, makes the activation method possible. Similarly to the case of ^{3}He(α,γ)^{7}Be, LUNA has measured this reaction with both in-beam and activation methods. The low-energy nonresonant cross section, as well as the strength of a narrow resonance of astrophysical importance, were measured with both techniques. The good agreement between the two approaches increased the reliability of the results in this case and led to precise reaction rates needed for astrophysical models (46, 47).

4.5.1.3. $^{12}C(p,\gamma)^{13}N$. The proton capture of ^{12}C is a part of the CNO cycle of hydrogen burning and strongly affects the ^{12}C/^{13}C isotopic ratio during stellar nucleosynthesis. LUNA is currently investigating this process. The short half-life of ^{13}N (9.965 min) necessitates an activation procedure different from what is discussed above. After irradiation, the target is not removed from the chamber, but instead, its activity is measured with the same detector as the one used for the in-beam γ spectroscopy. A combination of both approaches promises higher-precision and more reliable results than could be obtained by one approach alone.

4.5.2. Overground studies. The following cases provide examples of complementary studies performed both at overground and underground facilities.

4.5.2.1. $^{169}Tm(\alpha,\gamma)^{173}Lu$ and $^{144}Sm(\alpha,\gamma)^{148}Gd$. These two reactions play a role in the astrophysical p-process, which is the production mechanism of the heavy, proton rich, stable isotopes (48). The long half-life of the produced isotopes (1.37 and 71.1 y, respectively) allows for the separation of the irradiation and decay counting phases and associated measurement sites. The long half-lives result in low produced activities, which necessitate the application of an extremely low background counting setup. In the cases considered here, the irradiations were carried out at the cyclotron accelerator of ATOMKI in Debrecen, Hungary, and then the targets were transported to a low background detector at LNGS. The strongly improved detection limit of the underground facility allowed for the measurement of such low cross sections, which would not have been possible in an overground laboratory (49, 50).

p–p Chain: sequence of reactions converting H into ^{4}He; represents the main hydrogen burning mode in stars with $M \leq 1.3\ M_{\odot}$

Classical novae: stellar explosions driven by the thermonuclear runaway triggered on the surface of a white dwarf accreting H-rich material from a binary less-evolved companion

Big bang nucleosynthesis: network of reactions taking place soon after the big bang and leading to the synthesis of light elements such as deuterium, ^{3}He, ^{4}He, and ^{7}Li

Solar neutrino problem: factor-of-three discrepancy between the predicted and measured values of solar neutrinos flux on the Earth; finally solved by the discovery of neutrinos oscillations

4.5.2.2. ^{25}Mg(p,γ)^{26}Al. Although not an activation technique, the accelerator mass spectrometry (AMS) approach (51) must also be mentioned in this section, as it is also based on the direct detection of the reaction products and it, too, requires the reaction product to be radioactive. In an AMS experiment the number of produced isotopes is determined directly, not through their decay. Such an experiment does not require an underground location. However, it can be combined with in-beam γ spectroscopy performed underground. Such an experiment has been carried out by the LUNA collaboration for the study of the ^{25}Mg(p,γ)^{26}Al reaction (52), which plays a role in the Mg–Al cycle of advanced hydrogen burning. The irradiation and in-beam γ spectroscopy were performed at the LUNA 400-kV accelerator, while the AMS counting of the produced ^{26}Al isotopes was performed at the CIRCE AMS laboratory in Caserta, Italy. From the combination of the two methods, high-precision resonance strength values could be determined (53, 54).

5. THE LUNA LEGACY: 30 YEARS OF NUCLEAR ASTROPHYSICS UNDERGROUND

The LUNA collaboration has been pioneering underground nuclear astrophysics studies at the lowest energy frontiers for three decades. This work has led to unprecedented precision in the measurement of key reaction cross sections and to major breakthroughs in our understanding of the inner workings of stars. In the following, we present some key highlights from all the reactions studied so far. A full list, together with related astrophysical scenarios and experimental approaches, is given in **Table 2**.

5.1. Big Bang Nucleosynthesis

The BBN era has been explored at LUNA with two different experiments carried out with the LUNA 400-kV accelerator: ^{2}H(p,γ)^{3}He and ^{2}H(α,γ)^{6}Li. The results on the ^{2}H(p,γ)^{3}He reaction (discussed in more detail in Section 4.4.1) led to the most precise determination of the primordial deuterium abundance derived so far using BBN models (26). The ^{2}H(α,γ)^{6}Li cross section was related to the primordial ^{6}Li problem. Astronomical observations of primordial ^{6}Li in old stars find an abundance that is three orders of magnitude higher than expected according to BBN models. To solve this issue, it was suggested that ^{2}H(α,γ)^{6}Li (producing ^{6}Li) could have a resonance at low energies, increasing the cross section by orders of magnitude. At LUNA, the ^{2}H(α,γ)^{6}Li cross section was measured directly at BBN energies for the first time (59, 60). Since no resonance was found, such a reaction was ruled out as a possible solution to the ^{6}Li problem. It should be noted, however, that other—non-nuclear—solutions to the ^{6}Li problem also exist (see, e.g., 85, 86). Another nuclear reaction potentially related to the primordial ^{6}Li problem, and also linked to pre–main sequence hydrogen burning, is ^{6}Li(p,γ)^{7}Be. Prior to the LUNA measurement, its cross section was thought to have a broad resonance at $E_{cm} = 195$ keV. Its existence, however, was ruled out by a recent experiment at LUNA (65).

5.2. p–p Chain

Several experimental campaigns performed with the 50-kV and 400-kV accelerators shed light on a number of issues related to hydrogen burning in the Sun and other stars. The very first experiment carried out at LUNA was the measurement of the ^{3}He(^{3}He,2p)^{4}He cross section, which is part of the p–p chain. This cross section had never been measured within the solar Gamow window, and it could have potentially provided a solution to the solar neutrino problem. Indeed, the existence of a resonance in the solar Gamow energy region could shift reaction

Table 2 Overview of all reactions studied at LUNA to date

Reaction	Burning network	Studied energies (keV)	Target type	Detector/method	Reference(s)
$^{2}H(p,\gamma)^{3}He$	p–p Chain/BBN	2.5–22	Gas	4π-BGO	55
	BBN	32–263	Gas	HPGe	25, 26
$^{2}H(^{3}He,p)^{4}He$	p–p/e^{-} screening	4.2–13.8	Gas	Si	56–58
$^{2}H(\alpha,\gamma)^{6}Li$	BBN	80–133	Gas	HPGe	59, 60
$^{3}He(^{3}He,2p)^{4}He$	p–p Chain	16.5–24.4	Gas	Si	61–63
$^{3}He(\alpha,\gamma)^{7}Be$	p–p Chain/BBN	93–170	Gas	HPGe/activation	43–45, 64
$^{6}Li(p,\gamma)^{7}Be$	BBN, pre–main sequence	60–350	Solid	HPGe	65
$^{14}N(p,\gamma)^{15}O$	CNO	70–228	Gas	4π-BGO	66, 67
		119–370	Solid	HPGe	68–72
$^{15}N(p,\gamma)^{16}O$	CNO	90–230	Gas	4π-BGO	73
		70–375	Solid	HPGe/4π-BGO	74, 75
$^{17}O(p,\gamma)^{18}F$	CNO	167–370	Solid	HPGe/activation	46, 47
$^{17}O(p,\alpha)^{14}N$	CNO	E_R = 64.5, 183	Solid	Si	28, 30, 31, 76
$^{18}O(p,\gamma)^{19}F$	CNO	85–150	Solid	HPGe/4π-BGO	77, 78
$^{18}O(p,\alpha)^{15}N$	CNO	55–340	Solid	Si	29, 30
$^{22}Ne(p,\gamma)^{23}Na$	Ne-Na	68–300	Gas	HPGe/4π-BGO	20, 79–83
$^{22}Ne(\alpha,\gamma)^{26}Mg$	s-Process	E_R = 334	Gas	4π-BGO	D. Piatti et al., submitted manuscript
$^{23}Na(p,\gamma)^{24}Mg$	Ne-Na	E_R = 138, 240, 296	Solid	HPGe/4π-BGO	84
$^{24}Mg(p,\gamma)^{25}Al$	Mg-Al	E_R = 214	Solid	HPGe/4π-BGO	52
$^{25}Mg(p,\gamma)^{26}Al$	Mg-Al	E_R = 92, 130, 189, 304	Solid	HPGe/4π-BGO	52–54
$^{26}Mg(p,\gamma)^{27}Al$	Mg-Al	E_R = 326	Solid	HPGe/4π-BGO	52
$^{13}C(\alpha,n)^{16}O$	s-Process	230–300	Solid	^{3}He counter	37
$^{12}C(p,\gamma)^{13}N$	CNO	74–370	Solid	HPGe/activation	Ongoing
$^{13}C(p,\gamma)^{14}N$	CNO	74–371	Solid	HPGe/4π-BGO	Ongoing
$^{20}Ne(p,\gamma)^{21}Na$	Ne-Na	E_R = 366	Gas	HPGe	Ongoing

Energies are in the center-of-mass system. E_R indicates resonant energies. Abbreviations: BBN, big bang nucleosynthesis; BGO, bismuth germanate; HPGe, high-purity germanium.

sequence toward the first branch of the p–p chain, where no high-energy neutrinos are emitted, and therefore reconcile predictions of the solar neutrino flux with observations.

At LUNA, the $^{3}He(^{3}He,2p)^{4}He$ cross section was measured directly at solar Gamow energies, and no evidence for resonances was found (61–63). This experiment proved, for the first time, the potential of underground laboratories in nuclear astrophysics. The subsequent experiments at the 50-kV accelerator were still focused on solar physics [$^{2}H(p,\gamma)^{3}He$] (55) and on understanding the electron screening effect at low energies [$^{2}H(^{3}He,p)^{4}He$] (56–58).

The installation of the LUNA 400-kV accelerator in 2001 offered a sea of possibilities to explore reactions involving heavier nuclei and energy ranges of interest for stars more massive or more evolved than the Sun. The study of the p–p chain continued with the measurement of the $^{3}He(\alpha,\gamma)^{7}Be$ cross section (43–45, 64), required for a precise determination of the ^{7}Be neutrino flux from solar models.

5.3. CNO Cycle

CNO cycle: sequence of reactions converting H into He on preexisting CNO nuclides; represents the main hydrogen burning mode in stars with $M \geq 1.3\ M_{\odot}$

NeNa and MgAl cycles: Additional hydrogen burning cycles important for the synthesis of elements up to ^{27}Al, but with negligible energy contribution

Since 2001, the LUNA collaboration has been investigating most of the reactions occurring in the CNO cycle. These studies began with the ^{14}N(p,γ)^{15}O reaction, the slowest of the CNO cycle. Multiple experiments were performed (66–68, 70–72), targeting the Gamow window for shell hydrogen burning in AGB stars with unprecedented precision and improving cross section extrapolations into the solar Gamow window. With our improved LUNA data, the astrophysical reaction rate at temperatures below 100 MK was found to be 40% lower than the previously adopted literature value. Therefore, the expected CNO solar neutrino flux, as well as the nucleosynthesis calculations for AGB stars and classical novae, was revised. As a remarkable consequence, the age of galactic globular clusters, and by extension of the Universe, was increased by 0.7-1.0 Gy (69).

Following the success of the ^{14}N(p,γ)^{15}O experiments, many other crucial reactions of the CNO cycle were also studied at LUNA: namely, the ^{15}N(p,γ)^{16}O reaction, which initiates the NO loop of the cycle (73–75), and the (p,γ) and (p,α) branches on ^{17,18}O. The ratio of the ^{17}O(p,γ)^{18}F and ^{17}O(p,α)^{14}N cross sections determines the balance between the second and third CNO cycles and affects the isotopic abundances of oxygen and fluorine in AGB stars and classical novae (76).

In the ^{17}O(p,γ)^{18}F experiment, the reaction cross section was measured down to a center-of-mass energy of 167 keV, accessing for the first time the Gamow window for classical novae explosions. As mentioned in Section 4.5, this reaction was studied by both prompt γ-ray detection and activation techniques (46). Thanks to the consistent results obtained at LUNA, the uncertainty on the astrophysical reaction rate was reduced to 10%, a factor of four smaller than adopted in previous literature. This placed stronger constraints on the predicted abundances of key isotopes for novae nucleosynthesis, such as ^{18}F, ^{18}O, ^{19}F, and ^{15}N (47).

The study of the other reaction channel, ^{17}O(p,α)^{14}N, allowed for a new determination of the strength of the $E_p = 70$ keV resonance, which resulted in a factor-of-two increase in the astrophysical reaction rate at typical temperatures for intermediate-mass AGB stars (28) (see Section 4.4.2). The new proton capture rate of ^{17}O led to predicted ^{17}O/^{16}O isotopic ratios in better agreement with those observed in group II presolar grains, whose formation site was previously unknown. This solved a long-standing puzzle on the origin of these grains, revealing how stars of 4–8 $M_{\odot}$ can be a likely site for their production (31).

5.4. NeNa and MgAl Cycles

In addition to the CNO cycle, a detailed exploration of higher-temperature hydrogen burning through the NeNa and MgAl cycles was initiated at the LUNA 400-kV accelerator, investigating directly the relevant energies of red giant branch and AGB stars as well as classical nova explosions. In particular, among the reactions of the NeNa cycle, proton capture on ^{22}Ne (79, 82) and ^{23}Na (84) have already been investigated, while proton capture on ^{20}Ne is presently under study. Particularly notable are the results on the ^{22}Ne(p,γ)^{23}Na reaction, which used to be the most uncertain reaction of the NeNa cycle, with an uncertainty of up to three orders of magnitude on the astrophysical reaction rate. Several resonances contribute to the ^{22}Ne + p cross section, but none of the resonances below 400 keV had ever been observed in direct experiments, and only upper limits existed for their strengths (87).

In addition, the possible existence of three resonances at 71, 105, and 215 keV had only been tentatively reported by one experiment (88) but never observed in subsequent investigations (89). Two experimental campaigns were performed at LUNA (79, 80, 82), leading to the first observation of three resonances and their related γ-decay scheme. This study placed more stringent upper limits on the unobserved tentative resonances and allowed measurement of the direct capture contribution to the cross section down to unprecedented low energies. Thanks to the LUNA

data, the revised astrophysical reaction rate at AGB temperatures is now a factor of 10 higher than previously adopted (79), while its uncertainty has been reduced by at least two orders of magnitude.

Proton capture on ^{24,25,26}Mg was also studied at LUNA (52). Efforts were especially focused on the ^{25}Mg(p,γ)^{26}Al reaction, which produces radioactive ^{26}Al either in its ground state or in an isomeric state at 228 keV. While the isomeric state decays instantly into ^{26}Mg, the ground state decays with a half-life of 7×10^5 y, emitting a 1.809 MeV γ-ray, a signature of recent nucleosynthesis in our Galaxy. Two low-energy resonances of the ^{25}Mg(p,γ)^{26}Al reaction have been measured with unprecedented sensitivity (53). As a result, the new total reaction rate is about a factor of two higher than previously suggested, and the production rate of the isomeric state is up to a factor of five larger, with important consequences for the expected production sites of ^{26}Al (54).

s-Process nucleosynthesis: sequence of slow neutron-capture reactions (compared to characteristic β-decay lifetimes) contributing to the synthesis of elements heavier than iron

5.5. s-Process Nucleosynthesis

In the past few years, investigation of nuclear reactions involved in s-process nucleosynthesis has started at the LUNA 400-kV accelerator, and it will continue at the future LUNA MV machine (see Section 5.6). Two experiments have been performed so far: ^{13}C(α,n)^{16}O and ^{22}Ne(α,γ)^{26}Mg. The first reaction, discussed in Section 4.4.3, is one of the main neutron sources for the s-process, and LUNA provided direct cross section data within the Gamow window for the first time (37). The latter is the only open channel in ^{22}Ne+α fusion at low energies ($E < 565$ keV), while at higher energies the (α,γ) channel competes with the ^{22}Ne(α,n)^{25}Mg neutron source. The nucleosynthesis of isotopes between ^{26}Mg and ^{31}P in massive AGB stars is affected by the uncertainty of the ^{22}Ne(α,γ)^{26}Mg reaction rate (90). At temperatures below 0.3 GK, the ^{22}Ne(α,γ)^{26}Mg reaction rate is dominated by a weak resonance at 334 keV in the center of mass. Such resonance also affects the crossover temperature where the (α,n) rate starts to exceed the (α,γ) rate (90). The 334-keV resonance was tackled at LUNA using the gas target system and the 4π-BGO detector (D. Piatti et al., submitted manuscript).

5.6. Future Opportunities: LUNA MV

Despite the impressive progress of the past decades, many other important reactions remain beyond the reach of the existing LUNA 400-kV accelerator, partly because of the limitation to a maximum beam energy of 400 keV. This energy is typically enough for the study of most of the hydrogen burning reactions in or close to their Gamow windows. However, in those cases where the Gamow window cannot be reached, cross section measurements are needed over as wide an energy range as possible to aid theoretical extrapolations. Also, reactions of more advanced burning processes, such as, for example, helium and carbon burning, require even higher beam energies as they take place at correspondingly higher temperatures.

The need for a higher-energy accelerator deep underground at LNGS was formulated by the LUNA collaboration several years ago and also endorsed by NuPECC (91). The assessment of the technical requirements of the new accelerator and the careful selection of its location at LNGS have already been carried out, and 2021 finally witnessed the installation of the new LUNA MV machine. This project was funded by the Italian Ministry of Education, University and Research.

The LUNA MV accelerator is a single-ended inline Cockcroft–Walton accelerator with a maximum 3.5-MV terminal voltage. It was constructed by High Voltage Engineering Europa and optimized for high long- and short-term energy stability, long duty cycle, and long-term operation without personnel on site (92). It was installed on the north side of Hall B in the LNGS laboratory in a newly constructed, dedicated building that provides the necessary radiation shielding for the rest of the underground lab. The accelerator is able to deliver proton, α, and ^{12}C beams in the 300 keV-3.5 MeV energy range, with beam intensities up to 1,000, 500, and 150 eμA, respectively,

for the three ion species. By selecting the $^{12}C^{++}$ charge state, the energy range for the carbon beam can be extended to 7 MeV.

The LUNA collaboration has formulated a rich scientific program for the new accelerator in the coming years. The first reaction to be studied will be the $^{14}N(p,\gamma)^{15}O$ reaction, for which the collaboration already has extensive experience in its low-energy study at the 400-kV accelerator. Higher energy cross section measurements are needed, however, as the extrapolated cross section to solar energies is not precise enough for astrophysical models (42). These facts make the $^{14}N(p,\gamma)^{15}O$ reaction an ideal pilot project for LUNA MV. The cross section will be measured from the $E_p = 278$ keV resonance up to the maximum energy of the accelerator, providing a high-precision data set over a wide energy range overlapping with the available data from the LUNA 400-kV accelerator.

The availability of the carbon beam at LUNA MV will enable the study of the $^{12}C+^{12}C$ reaction, arguably one of the most important in nuclear astrophysics as it regulates energy generation and nucleosynthesis during the carbon burning phase of massive stars (93) and dictates whether they will explode as supernovae. Cross section data available in the literature often present inconsistencies and, in addition, do not reach low enough energies (94). At the LUNA MV accelerator, the proton and α channels of the reaction will be measured—supplemented by the detection of γ-rays from the excited states of residual nuclei—at energies lower than ever before, including the search for possible low-energy resonances.

A natural continuation of the $^{13}C(\alpha,n)^{16}O$ cross section measurement already performed at the LUNA 400-kV accelerator foresees the higher-energy study of both s-process neutron-source reactions, $^{13}C(\alpha,n)^{16}O$ and $^{22}Ne(\alpha,n)^{25}Mg$. The complicated structure of the $^{13}C(\alpha,n)^{16}O$ excitation function and the uncertain overall normalization require cross section measurements over a broad energy range. This will be achieved with a setup similar to the one used at the LUNA 400-kV accelerator. The possibility of using inverse kinematics has also been considered, which would likely afford conditions of reduced beam-induced background. The $^{22}Ne(\alpha,n)^{25}Mg$ reaction is the main source of neutrons for the s-process in massive stars. For its study, a novel type of neutron detector will be developed as part of an ERC project, SHADES (Scintillator-^{3}He Array for Deep-underground Experiments on the S-process). The new detector array, combined with the ultra-low background environment and the high beam intensity of LUNA MV, will allow for the measurement of high-accuracy cross sections about two orders of magnitude lower than previously achieved for this reaction. Exploring the whole Gamow window will drastically reduce the uncertainty of the astrophysical reaction rate in the relevant temperature range.

6. OTHER UNDERGROUND LABORATORIES WORLDWIDE

Not surprisingly, the success story demonstrated by the pioneering work at LUNA has prompted worldwide efforts for the installation of similar accelerators in other underground laboratories. Some of these initiatives are briefly presented in the next section.

6.1. CASPAR, United States

CASPAR, the Compact Accelerator System for Performing Astrophysical Research, was the first accelerator to be commissioned at an underground site in the United States. Located at the Sanford Underground Research Facility in the former Homestake gold mine (Lead, South Dakota) it was designed for nuclear astrophysics measurements at a depth of 4,850 ft (1,478 m), affording shielding against cosmic radiation of about 4,300 m.w.e. (95). Its 1-MV Van de Graaff accelerator already had a fruitful history in research starting long before CASPAR (96). After

upgrades to increase the beam intensity and modernize the control system, the accelerator was installed at SURF, where first beam was produced in 2017 (95).

With an operational range of 150 kV to 1,100 kV terminal voltage (97) and beam intensities of up to 250 μA, CASPAR extended the available energy range for proton and helium beams at underground facilities, previously set by the LUNA 400-kV accelerator, and thus opened up opportunities for new underground studies. With the availability of a solid target and a windowless gas target setup, a wide range of reactions can now be studied at CASPAR. As a commissioning experiment, ^{14}N(p,γ)^{15}O was studied using solid targets. HPGe or high-efficiency NaI(Tl) detection setups are available for the study of radiative capture reactions, complemented by an array of ^{3}He counters for neutron detection. More recent measurements include those of ^{10}B(α,n)^{14}N and ^{7}Li(α,γ)^{11}B (97), as well as ^{22}Ne(α,n)^{26}Mg (98). Data analysis is currently in progress. A rich scientific program is planned for the study of key reactions at CASPAR, complementing the capabilities of the other underground accelerator facilities.

6.2. JUNA, China

The Jinping Underground Nuclear Astrophysics (JUNA) laboratory is located in the Sichuan province, China, under the Jinping mountain, which provides a shielding of 2,400 m (7,620 m.w.e.) of radioactively quiet marble rocks and affords a cosmic-ray background two orders of magnitude lower than at Gran Sasso (99). A 400-kV accelerator, coupled to a 2.45-GHz electron cyclotron resonance source, is capable of delivering up to 12-emA proton and 6-emA ^{4}He^{+} beams (99). Space charge effects and beam transport efficiency are optimized by the use of a low-energy beam transport line. The accelerator started operation in December 2020, and four experiments have already been performed (97), as briefly summarized below.

The ^{12}C(α,γ)^{16}O reaction, which regulates the C/O abundance at the end of helium burning and affects the subsequent phases of stellar evolution, was studied in direct kinematics using a 1-emA ^{4}He^{+} beam onto a pure ^{12}C target surrounded by an array of BGO and LaBr detectors; the reaction cross section was measured down to $E_{cm} = 600$ keV, the lowest to date. The ^{13}C(α,n)^{16}O reaction, the main source of neutrons for the s-process in AGB stars at temperatures $T = 90$ MK, was studied down to $E_{cm} = 400$–600 keV using intense (0.1–2 pmA) beams of ^{4}He^{+} and ^{4}He^{++} on 2-mm-thick ^{13}C targets; neutrons were detected with an array of 24 ^{3}He counters arranged in concentric rings. Measurements of the ^{25}Mg(p,γ)^{26}Al reaction, important for the synthesis of ^{26}Al in the Galaxy, have focused on the width of two important resonances at 92 and 189 keV (100). Thick target yield measurements were performed using a 4π-BGO γ-ray detector. Finally, the ^{19}F(p,$\alpha\gamma$)^{16}O and ^{19}F(p,γ)^{20}Ne reactions, important in the CNO cycle, were studied in a combination of overground and underground measurements, the latter extending down to $E_{cm} =$ 72 keV and 188 keV for the two reactions, respectively. A new resonance, observed at 225 keV in ^{19}F(p,γ)^{20}Ne, enhances the rate by a factor of four, thus increasing leakage from the CNO cycle and possibly explaining Ca abundance in the first-generation population III stars (97). Results from the ^{19}F(p,$\alpha\gamma$)^{16}O study were recently published (101). The scientific program at JUNA is expected to continue, with the potential for major breakthroughs in nuclear astrophysics research.

6.3. Felsenkeller, Germany

Unlike the deep underground laboratories described above, the Felsenkeller ion accelerator laboratory in Dresden, Germany, is a shallow underground site (**https://www.hzdr.de/db/Cms?pNid=1029**). It is located under 45 meters of hornblende monzonite rock overburden (140 m.w.e.). Such a depth is enough to completely shield all the components of cosmic-ray-induced radiations except muons. The significant remaining muon flux necessitated a detailed

study of the background conditions of the site and the optimization of detection techniques. Dedicated experiments were devoted to assess γ-ray (102), neutron (103), and muon backgrounds (104). An important conclusion was that the combination of the shallow underground location with active detector shielding results in a background rate in γ detectors that is only a factor of 2–3 worse than in a deep underground laboratory at γ-ray energies of 5-8 MeV (105). Such a background is low enough for nuclear astrophysics studies, and a shallow underground accelerator can be a good alternative or a complementary facility to deep underground ones. Thanks to these encouraging results, a 5-MV Pelletron tandem accelerator has recently been installed at the Felsenkeller laboratory. Thanks to the additional ion source on the high-voltage terminal, the accelerator can be used in both tandem and single-ended modes and can deliver proton, α particle, and ^{12}C ion beams with several tens of μA intensity.

The scientific program of the Felsenkeller underground ion accelerator laboratory (106) anticipates the study of several reactions of astrophysical importance, such as $^{3}\mathrm{He}(\alpha,\gamma)^{7}\mathrm{Be}$ and $^{12}\mathrm{C}(\alpha,\gamma)^{16}\mathrm{O}$. To fully exploit the background reduction capabilities, a number of HPGe detectors surrounded by active veto detectors will be used for the experiments.

7. CONCLUSIONS AND OUTLOOK

The past few decades have witnessed tremendous developments in astronomy and astrophysics. Astronomical observations have become astoundingly precise, and supercomputers now allow detailed 3D modeling of stellar interiors at various stages of stellar evolution. As a result, we have a better understanding of astrophysical phenomena and a deeper knowledge of the elemental composition of the universe. Yet, improved descriptions of microscopic processes in stars are also needed. Nuclear reactions generate the energy of stars and produce the chemical elements, so knowing the characteristics of these reactions is necessary in modern astrophysics.

Since the birth of nuclear astrophysics in the middle of the twentieth century, many fusion reactions between stable nuclei have been studied experimentally, leading to a broad understanding of stellar evolution and nucleosynthesis. However, the extremely low cross sections encountered at stellar temperatures long prevented the study of reactions directly at the relevant energies. Cutting-edge experimental techniques are needed for such studies and require intense ion beams, high-efficiency detection systems, and modern nuclear electronics. Background radiation from environmental radioactivity or of cosmic origin may still hinder the measurement of low cross sections. The effective reduction of the background is thus critically important.

The most effective suppression of cosmic-ray-induced background can be achieved by placing the experiment in a deep underground laboratory shielded by hundreds to thousands of meters of rock. In the past 30 years, the LUNA collaboration—which, for a long time, operated the world's only deep underground accelerator—proved that a deep location combined with advanced experimental techniques can lead to measured cross sections much lower and much more precise than previously achieved.

In this article, we have summarized the experimental requirements and solutions for a successful measurement of low reaction cross sections in an underground laboratory. The methods used by the LUNA collaboration served as examples, and highlights of key scientific achievements have been presented. However, the fast development of observational and theoretical astrophysics necessitates further progress in experimental nuclear astrophysics. There are many cases where nuclear cross sections represent the major source of uncertainty in stellar models. The unique conditions offered by an underground accelerator need to be further exploited to improve the nuclear physics input of astrophysical calculations. The upgrade of the LUNA project to a

higher-energy accelerator is imminent, and other worldwide initiatives for deep underground nuclear astrophysics experiments have recently become operational. These facilities will help nuclear physics to keep pace with the high-precision observations in astrophysics.

SUMMARY POINTS

1. Thermonuclear reactions in stars take place over a narrow energy region commonly referred to as the Gamow peak. The peak curve arises from the product of the Maxwell–Boltzmann distribution at a given stellar temperature T and the quantum probability of tunneling through the Coulomb barrier between the interacting nuclei.
2. The cross sections of thermonuclear reactions drop exponentially at Gamow energies and are extremely challenging to study in terrestrial laboratories.
3. Underground laboratories, with their significantly reduced cosmic-ray backgrounds, provide an ideal environment to study nuclear reactions of astrophysical interest.
4. Major progress has been achieved at the Laboratory for Underground Nuclear Astrophysics (LUNA) located under the Gran Sasso mountain in Italy. The 1.4-km rock overburden affords significantly reduced backgrounds for the detection of γ-rays, charged particles, and neutrons.
5. Over the past 30 years, the LUNA collaboration has studied key hydrogen burning reactions relevant to big bang nucleosynthesis, the p–p chain, the CNO cycle, and the NeNa and MgAl cycles. These studies have led to an improved understanding of energy generation and nucleosynthesis in various astrophysical sites, including the Sun, red giant and asymptotic giant branch stars, and classical novae.

FUTURE ISSUES

1. Despite the impressive progress achieved so far, many key reactions of astrophysical interest remain beyond technical capabilities at the existing LUNA 400-kV accelerator.
2. A new 3.5-MV accelerator recently installed at Gran Sasso will open up unprecedented opportunities for the study of key nuclear reactions of helium and carbon burning, including the two neutron sources, $^{13}C(\alpha,n)^{16}O$ and $^{22}Ne(\alpha,n)^{25}Mg$, and the $^{12}C(^{12}C,p)^{23}Na$ and $^{12}C(^{12}C,\alpha)^{20}Ne$ reactions. A further study, $^{14}N(p,\gamma)^{15}O$, is also planned during the commissioning of the new accelerator and will serve to investigate the core metallicity of the Sun. These studies will help shed light on more advanced stages of the evolution of massive stars.
3. New underground laboratories dedicated to nuclear astrophysics studies have become operational in recent years, both in the United States (CASPAR) and in China (JUNA). Initial scientific results have recently been published.
4. Shallow underground laboratories, such as Felsenkeller, do not offer the same level of background suppression as deep underground laboratories and generally necessitate active veto detectors. Nevertheless, they provide a useful complementary site for the study of astrophysical reactions for which background issues are not the limiting factor.

DISCLOSURE STATEMENT

The authors are not aware of any affiliations, memberships, funding, or financial holdings that might be perceived as affecting the objectivity of this review.

ACKNOWLEDGMENTS

This work was supported, in part, by the Science and Technology Facilities Council, UK (grant no. STFC ST/P004008/1), and by National Research, Development and Innovation Office (NKFIH) grant no. K134197. M.A. also acknowledges financial support from the ExtreMe Matter Institute during her Visiting Professorship at GSI/Goethe University Frankfurt. A.B. received funding from the European Union under European Research Council (ERC) grant agreement 852016 (SHADES) and grant agreement 101008324 (ChETEC-INFRA). For the purpose of open access, the authors have applied a Creative Commons Attribution (CC BY) license to any Author Accepted Manuscript version arising from this submission.

LITERATURE CITED

1. Abbott BP, et al. *Phys. Rev. Lett.* 116(6):061102 (2016)
2. Bartos I, Kowalski M. *Multimessenger Astronomy*. Bristol, UK: IOP Publ. (2017)
3. Burbidge EM, Burbidge GR, Fowler WA, Hoyle F. *Rev. Mod. Phys.* 29(4):547–650 (1957)
4. Cameron A. *Publ. Astron. Soc. Pac.* 69(408):201–22 (1957)
5. Rolfs C, Rodney W. *Cauldrons in the Cosmos: Nuclear Astrophysics*. Chicago: Univ. Chicago Press (1988)
6. Descouvemont P, Baye D. *Rep. Prog. Phys.* 73(3):036301 (2010)
7. Assenbaum HJ, Langanke K, Rolfs C. *Z. Phys. A* 327(4):461–68 (1987)
8. Gyürky G, et al. *Phys. Rev. C* 100(1):015805 (2019)
9. Ciani GF, et al. *Eur. Phys. J. A* 56(3):75 (2020)
10. Formicola A, et al. *Nucl. Instrum. Methods Phys. Res. A* 507(3):609–16 (2003)
11. Rajta I, et al. *Nucl. Instrum. Methods Phys. Res. A* 880:125–30 (2018)
12. Marta M, et al. *Nucl. Instrum. Methods Phys. Res. A* 569(3):727–31 (2006)
13. Bemmerer D, et al. *Europhys. Lett.* 122(5):52001 (2018)
14. Cuesta C, et al. *Opt. Mater.* 36(2):316–20 (2013)
15. Caciolli A, et al. *Eur. Phys. J. A* 48:144 (2012)
16. Champagne AE, Iliadis C, Longland R. *AIP Adv.* 4(4):041006 (2014)
17. Depalo R, et al. *INFN-LNL Rep.* 262:97 (2021)
18. Iliadis C. *Nuclear Physics of Stars*. New York: Wiley (2007)
19. Greife U, et al. *Nucl. Instrum. Methods Phys. Res. A* 350(1):327–37 (1994)
20. Cavanna F, et al. *Eur. Phys. J. A* 50:179 (2014)
21. Aghanim N, et al. *Astron. Astrophys.* 641:A6 (2020)
22. Ma L, et al. *Phys. Rev. C* 55(2):588–96 (1997)
23. Tišma I, et al. *Eur. Phys. J. A* 55(8):137 (2019)
24. Marcucci LE, Mangano G, Kievsky A, Viviani M. *Phys. Rev. Lett.* 116(10):102501 (2016)
25. Mossa V, et al. *Eur. Phys. J. A* 56(5):144 (2020)
26. Mossa V, et al. *Nature* 587(7833):210–13 (2020)
27. Misiaszek M, et al. *Appl. Radiat. Isot.* 81:146–50 (2013)
28. Bruno CG, et al. *Phys. Rev. Lett.* 117(14):142502 (2016)
29. Bruno C, et al. *Phys. Lett. B* 790:237–42 (2019)
30. Bruno CG, et al. *Eur. Phys. J. A* 51:94 (2015)
31. Lugaro M, et al. *Nat. Astron.* 1:0027 (2017)
32. Heusser G. *Annu. Rev. Nucl. Part. Sci.* 45:543–90 (1995)
33. Belli P, et al. *Nuovo Cimento A* 101(6):959–66 (1989)
34. Best A, et al. *Nucl. Instrum. Methods Phys. Res. A* 812:1–6 (2016)

35. Bruno G, Fulgione W. *Eur. Phys. J. C* 79(9):747 (2019)
36. Csedreki L, et al. *Nucl. Instrum. Methods Phys. Res. A* 994:165081 (2021)
37. Ciani GF, et al. *Phys. Rev. Lett.* 127(15):152701 (2021)
38. Balibrea-Correa J, et al. *Nucl. Instrum. Methods Phys. Res. A* 906:103–9 (2018)
39. Drotleff HW, et al. *Astrophys. J.* 414:735 (1993)
40. Heil M, et al. *Phys. Rev. C* 78(2):025803 (2008)
41. Gyürky G, et al. *Eur. Phys. J. A* 55(3):41 (2019)
42. Adelberger EG, et al. *Rev. Mod. Phys.* 83(1):195–245 (2011)
43. Bemmerer D, et al. *Phys. Rev. Lett.* 97(12):122502 (2006)
44. Gyürky G, et al. *Phys. Rev. C* 75(3):035805 (2007)
45. Confortola F, et al. *Phys. Rev. C* 75(6):065803 (2007)
46. Scott DA, et al. *Phys. Rev. Lett.* 109(20):202501 (2012)
47. Di Leva A, et al. *Phys. Rev. C* 89(1):015803 (2014)
48. Rauscher T, et al. *Rep. Prog. Phys.* 76(6):066201 (2013)
49. Kiss GG, et al. *Nucl. Phys. A* 867(1):52–65 (2011)
50. Somorjai E, et al. *Astron. Astrophys.* 333:1112–16 (1998)
51. Kutschera W. *Adv. Phys. X* 1(4):570–95 (2016)
52. Limata B, et al. *Phys. Rev. C* 82(1):015801 (2010)
53. Strieder F, et al. *Phys. Lett. B* 707(1):60–65 (2012)
54. Straniero O, et al. *Astrophys. J.* 763(2):100 (2013)
55. Casella C, et al. *Nucl. Phys. A* 706(1):203–16 (2002)
56. Prati P, et al. *Z. Phys. A* 350(2):171–76 (1994)
57. Costantini H, et al. *Phys. Lett. B* 482(1):43–49 (2000)
58. Zavatarelli S, et al. *Nucl. Phys. A* 688(1):514–17 (2001)
59. Anders M, et al. *Phys. Rev. Lett.* 113(4):042501 (2014)
60. Trezzi D, et al. *Astropart. Phys.* 89:57–65 (2017)
61. Arpesella C, et al. *Phys. Lett. B* 389(3):452–56 (1996)
62. Junker M, et al. *Phys. Rev. C* 57(5):2700–10 (1998)
63. Bonetti R, et al. *Phys. Rev. Lett.* 82(26):5205–8 (1999)
64. Costantini H, et al. *Nucl. Phys. A* 814(1):144–58 (2008)
65. Piatti D, et al. *Phys. Rev. C* 102(5):052802 (2020)
66. Bemmerer D, et al. *Nucl. Phys. A* 779:297–317 (2006)
67. Lemut A, et al. *Phys. Lett. B* 634(5):483–87 (2006)
68. Formicola A, et al. *Phys. Lett. B* 591(1):61–68 (2004)
69. Imbriani G, et al. *Astron. Astrophys.* 420:625–29 (2004)
70. Imbriani G, et al. *Eur. Phys. J. A* 25(3):455–66 (2005)
71. Marta M, et al. *Phys. Rev. C* 78(2):022802 (2008)
72. Marta M, et al. *Phys. Rev. C* 83(4):045804 (2011)
73. Bemmerer D, et al. *J. Phys. G.* 36(4):045202 (2009)
74. LeBlanc PJ, et al. *Phys. Rev. C* 82(5):055804 (2010)
75. Caciolli A, et al. *Astron. Astrophys.* 533:A66 (2011)
76. Straniero O, et al. *Astron. Astrophys.* 598:A128 (2017)
77. Best A, et al. *Phys. Lett. B* 797:134900 (2019)
78. Pantaleo FR, et al. *Phys. Rev. C* 104(2):025802 (2021)
79. Cavanna F, et al. *Phys. Rev. Lett.* 115(25):252501 (2015)
80. Depalo R, et al. *Phys. Rev. C* 94(5):055804 (2016)
81. Slemer A, et al. *Mon. Not. R. Astron. Soc.* 465(4):4817–37 (2016)
82. Ferraro F, et al. *Phys. Rev. Lett.* 121(17):172701 (2018)
83. Ferraro F, et al. *Eur. Phys. J. A* 54(3):44 (2018)
84. Boeltzig A, et al. *Phys. Lett. B* 795:122–28 (2019)
85. Lind K, et al. *Astron. Astrophys.* 554:A96 (2013)
86. Steffen M, et al. *Mem. Soc. Astron. Ital. Suppl.* 22:152 (2012)

87. Iliadis C, et al. *Nucl. Phys. A* 841(1):31–250 (2010)
88. Powers JR, Fortune HT, Middleton R, Hansen O. *Phys. Rev. C* 4:2030–46 (1971)
89. Hale SE, et al. *Phys. Rev. C* 65:015801 (2001)
90. Karakas AI, et al. *Astrophys. J.* 643(1):471–83 (2006)
91. NuPECC. **http://nupecc.org/pub/lrp17/lrp2017.pdf** (2017)
92. Sen A, et al. *Nucl. Instrum. Methods Phys. Res. B* 450:390–95 (2019)
93. Beck C, Mukhamedzhanov AM, Tang X. *Eur. Phys. J. A* 56(3):87 (2020)
94. Tan WP, et al. *Phys. Rev. Lett.* 124(19):192702 (2020)
95. Heise J. *J. Phys. Conf. Ser.* 1342:012085 (2020)
96. Wiescher M. *Phys. Perspect.* 19(2):151–79 (2017)
97. Aliotta M, et al. *J. Phys. G.* 49:010501 (2022)
98. Strieder F, et al. In *Nuclei in the Cosmos XV*, ed. A Formicola, M Junker, L Gialanella, G Imbriani, pp. 259–63. New York: Springer (2019)
99. Liu W, et al. *Sci. China Phys. Mech. Astron.* 59(4):642001 (2016)
100. Su J, et al. *Sci. Bull.* 67:125–32 (2022)
101. Zhang L, et al. *Phys. Rev. Lett.* 127:152702 (2021)
102. Szücs T, et al. *Eur. Phys. J. A* 55(10):174 (2019)
103. Grieger M, et al. *Phys. Rev. D* 101(12):123027 (2020)
104. Ludwig F, et al. *Astropart. Phys.* 112:24–34 (2019)
105. Szücs T, et al. *Eur. Phys. J. A* 48(1):8 (2012)
106. Bemmerer D, et al. In *Solar Neutrinos*, ed. K Zuber, M Meyer, pp. 249–63. Singapore: World Sci. (2019)

Annual Review of Nuclear and Particle Science

Volume 72, 2022

Contents

Errata

An online log of corrections to *Annual Review of Nuclear and Particle Science* articles may be found at http://www.annualreviews.org/errata/nucl